Stability characteristics of shallow landslide triggered by rainfall

Avirut CHINKULKIJNIWAT[1]* https://orcid.org/0000-0003-4905-7991; ✉ e-mail: avirut@sut.ac.th

Taworn TIRAMETATIPARAT[1] https://orcid.org/0000-0001-5027-5537; e-mail: D5840519@g.sut.ac.th

Chanathip SUPOTAYAN[1] https://orcid.org/0000-0001-8289-4666; e-mail: ch.supotayan@gmail.com

Somjai YUBONCHIT[1,2] https://orcid.org/0000-0003-3434-9537; e-mail: d5540150@g.sut.ac.th

Suksun HORPIBULSUK[1] https://orcid.org/0000-0003-1965-8972; e-mail: suksun@g.sut.ac.th

Rattana SALEE[1] https://orcid.org/0000-0001-5411-399X; e-mail: saleerattana6155@gmail.com

Panich VOOTTIPRUEX[3] https://orcid.org/0000-0002-9474-2915; e-mail: pnv@fte.kmutnb.ac.th

* Corresponding author

1 School of Civil Engineering, Center of Excellence in Civil Engineering, Institute of Engineering, Suranaree University of Technology, Nakhon Ratchasima 30000, Thailand

2 Department of Civil Engineering, Rajamangala University of Technology Isan, Nakhon Ratchasima 30000, Thailand

3 Department of Teacher Training in Civil Engineering, King Mongkut's University of Technology North Bangkok 10800, Thailand

Citation: Chinkulkijniwat A, Tirametatiparat T, Supotayan C, et al. (2019) Stability characteristics of shallow landslide triggered by rainfall. Journal of Mountain Science 16(9). https://doi.org/10.1007/s11629-019-5523-7

Abstract: Rainfall-induced shallow landslides are known to be extremely dangerous since the sliding mass can propagate quickly and travel far from the source. Although the sliding mechanism in sloping ground is simple to understand, the problem may be complicated by unsaturated transient water flow. The flow behavior of rainwater in unsaturated sloping ground and the consequent factor of safety must be clearly understood to assess slope stability under rainfall conditions. A series of laboratory experiments was conducted to examine the critical hydrological states so that assessment of slope stability under rainfall condition can be performed. Based on the test results, a unique relationship between critical hydrological states, rainfall intensity, and soil properties was formulated. Sequential stability analysis provided insights into the stability of slopes subjected to variations in soil properties, slope angles and rainfall intensities, and the consequent variation in the depth of the failure plane, vital in landslide risk assessment, was determined through this analysis. The variation of rainfall intensity was found to strongly affect the depth of the failure plane in cohesionless sloping ground. Furthermore, the influence of rainfall intensity on the depth of the failure plane may be alleviated by a small magnitude of cohesive strength. The results of this study will reinforce knowledge of landslide behavior and help to improve mitigation measures in susceptible areas.

Keywords: Shallow landslides; Rainfall; Failure depth

Introduction

Rainfall-induced landslides are natural disasters that are encountered in many parts of the world and they always result in massive destruction and loss of human life (Yumuang 2006; Guzzeti et al. 2008). Among the various types of landslides, shallow landslides present a special danger since they can potentially initiate debris flow (Trustrum et al. 1999), particularly when rainfall continues after the initiation of the failure. The huge scale of damage caused by shallow landslides has been reported in the literature (Gabet and Mudd 2006; Postance et al. 2018). Shallow landslides are typically translational slope failures that involve the upper few meters of unconsolidated surficial material. Recent reports (Li et al. 2013; Chinkulkijniwat et al. 2016; Yubonchit et al. 2016; Naidu et al. 2018) have concluded that, for rainfall-induced translational slides in terrains of homogeneous soil, the sliding failure can be categorized as occurring in two major phases: the infiltration phase and the saturation phase. In the infiltration phase, rainwater infiltrates the sloping ground advancing the wetting zone. If the failure takes place in this phase, the failure plane can occur at any depth depending on factors such as the slope angle, rainfall intensity, and soil properties. The saturation phase takes place during the rising of the water table, which initially occurs after rainwater reaches the impermeable interface. In this phase, the failure plane occurs only at the impervious interface.

The ability to predict the depth of the failure plane is vital when assessing slope stability during a rainfall event. A number of reports (Shimoma et al. 2002; Chaminda 2006; Tohari et al. 2007) found that slope failure is initiated at the slope toe since the fully saturated condition of soil at this position results in the development of excessive positive pore water pressure. However, their findings were based on homogeneous soil slopes, where the dominant failure mode will be a circular or noncircular sliding failure. Although the danger of shallow landslides has been recognized, reports that focused on the depth of the failure plane in shallow landslides have been limited in number (Tsai et al. 2008; Li et al. 2013; Ali et al. 2014; Chinkulkijniwat et al. 2016) and few attempted a rigorous understanding of the stability characteristics of shallow landslides.

Chinkulkijniwat et al. (2016) were among the few to attempt a characterization of the stability of shallow landslides that took multiple factors into account. They conducted a series of artificial rainwater infiltration tests and introduced a mathematical model to approximate the magnitude of water content in sloping ground subjected to a certain magnitude of rainfall intensity. This approximated water content was used to create a profile of the factor of safety of a sloping terrain subjected to various magnitudes of rainfall intensity. Subsequently, they developed a critical depth chart based on relationships between the depth of the failure plane, the rainfall intensity and the steepness of various slopes. The stability of shallow slopes was then characterized via the critical depth chart and, using this chart, the possible depth of the failure plane was comprehensively defined. They reported that the depth of the failure plane can be determined from the soil frictional angle (ϕ'), the soil saturated permeability (k_s), the steepness of the slope (β), and the rainfall intensity (i). However, the conclusions of Chinkulkijniwat et al. (2016) were limited to cohesionless sandy soil possessing no fine fraction. Soils in mountainous terrain typically possess both a certain amount of fine fraction and either intrinsic cohesive strength or apparent cohesive strength, especially due to plant roots, which reinforce soil by their tensile strength and adhesion properties to form enclosed root matrix systems that give soil additional apparent cohesion (Tosi 2007; Burylo et al. 2011). Failure characteristics of these soils might well differ from those of cohesionless sandy soil.

To further knowledge of the stability characteristics of sloping grounds, this study extends the work of Chinkulkijniwat et al. (2016) to soils that contain a certain amount of fine fraction and possess cohesive strength. The work extended the analysis of the critical depth charts for various soil types so that a comparison among the stability characteristics of different soils could be thoroughly interpreted. The study began with a series of laboratory tests to clarify the hydrological behavior of the studied soils and, based on the conclusions drawn for hydrological behavior, continued by analyzing the stability of the soils using the infinite slope model under various

rainfall intensities. Results from this study will reinforce related research that seeks to design landslide mitigation measures.

1 Hydrological State at the Wetting Front

For a ponded surface, the maximum water content during the infiltration phase is equal to the saturated water content, Green and Ampt (1911). However, in the case of an unponded surface, although Mein and Larson (1973) and Chu (1978) elaborated the model proposed by Green and Ampt (1911), they did not clearly elaborate the maximum magnitude of water content during the infiltration process, which in the present work is termed water content behind the wetting front, θ_{wb}. Mostly, the saturated water content was assumed without consideration of rainfall intensity and soil hydrological properties. Chinkulkijniwat et al. (2016) reported a unique relationship between θ_{wb} and the infiltration index (i/k_s), defined as the rainfall intensity (i) over the saturated soil permeability (k_s), regardless of the slope gradient and initial water content. However, their report was based only on test results from a cohesionless sand, which were considered to have distinct (or sharp) wetting front characteristics. In this work, the relationship between θ_{wb} and i/k_s found in Chinkulkijniwat et al. (2016) was further validated with two soils that possessed a certain amount of fine fraction. Furthermore, the water content (θ_w) profile of studied soils that possessed a certain amount of fine fraction was revisited to test the validity of the proposed sharp wetting front boundary during various rainfall intensities.

1.1 Laboratory tests and experimental setup

The two soils used in this study contained a certain amount of fine fraction. The soil water characteristic (SWC) curve of the studied soils was determined in accordance with the ASTM D6836-02. The air-dried soils were compacted to the retainer rings placed on a saturated ceramic plate in the pressure chamber. Saturation state was acquired by spraying water from above the soil specimens. After being encapsulated, the airtight pressure chamber was subjected to a specific air pressure in order to push the water out of the specimens. The air pressure was kept constant until no more water was released from the chamber. The specimens were then placed into the oven to determine their water content. The above procedures were repeated for various magnitudes of air pressure. The dataset between air pressure and soil water content was used to plot the SWC curve of the studied soils. Shear strength parameters were determined from the direct shear test (ASTM D3080). Each studied soil was compacted to three identical density specimens. Direct shear testing was conducted under three normal stress levels of 50,100 and 200 kPa with a 1 mm/min displacement rate. The strength parameters (φ' , c') were acquired from the peak shear stress values of shear stress-horizontal displacement plots.

A series of infiltration tests were carried out in a one-dimensional column to simulate infiltration processes in the studied soils, which were later classified as SM and SM-SP soils. Figure 1 shows the schematic diagram, dimensions and a photograph of the one-dimensional soil infiltration test apparatus. The apparatus consisted of a rainfall simulator, a steel frame and an experiment column. The experiment column was made from an acrylic tube 100 mm in diameter and 1000 mm in height. An impervious acrylic plate 15 mm thick was used as the base of the experiment column. Five holes of 5 mm diameter were made in the column 100, 200, 300, 400, and 500 mm from the base. These were for the installation of moisture sensor probes. To ensure homogeneity, 7728 grams of SM soil and 8247 grams of SP-SM soil were dried in air before being layered into the standing pipe column. Ten compacted layers 60 mm thick were put in place to create a column of soil 0.6 m high. The unit weight of the SM soil and SP-SM soil columns was 16.4 kN/m³ and 17.5 kN/m³, respectively. Five moisture sensor probes (Decagon 5TE, Decagon Devices Inc. (2007-2010)) and a piezometer were then installed. The piezometer was placed in the base of the column. An open valve was also placed in base of the column close to the piezometer to prevent the occurrence of trapped air during the tests. Rainwater infiltration tests were conducted by assigning the desired intensities of rainfall to the experiment column. The desired rainfall intensities were assigned through a well-calibrated rainfall simulator comprising a water tank, a constant

water pressure pump, a pressure gauge, a plastic pipe, a control valve, and a fine spray nozzle placed in the plastic pipe.

The experimental program is summarized in Table 1. The magnitudes of rainfall intensity used in the experiment were determined by the saturated permeability of the studied soils. Rainfall intensities of 5, 10, 20, and 45 mm/hr were assigned to the SM column, whose saturated permeability was 15 mm/hr (k_{sat} = 4.167 × 10^{-6} m/sec ≈ 15 mm/hr). Rainfall intensities of 10, 20, 45, 70 and 100 mm/hr were applied to the SP-SM column, whose saturated permeability was 65 mm/hr (k_{sat} = 1.806 × 10^{-5} m/sec ≈ 65 m/hr). These variations were applied to demonstrate the hydrological responses under three rainfall conditions: rainfall intensity lower than the soil saturated permeability ($i < k_s$), rainfall intensity approaching the soil saturated permeability ($i \approx k_s$), and rainfall intensity greater than the soil saturated permeability ($i > k_s$). In each rainfall test, rainfall was applied until the steady state was reached. The onset of the steady state was indicated when the values for water content remained constant at all moisture sensors.

1.2 Test results

The grain-size distribution and SWC curves of the studied soils are respectively presented in

Table 1 Infiltration tests in one-dimensional column conducted in this study

Soil property		Value	
Soil type (USCS classification)		SM	SP-SM
% Clay		2	1
% Silt		36	10
% Sand		62	89
Atterberg's limits			
Liquid limit, LL (%)		19.80	NP
Plastic limit, PL (%)		14.95	NP
Plasticity index, PI (%)		4.85	NP
Specific gravity, G_s		2.59	2.62
Dry unit weight, γ_d (kN/m³)		16.4	17.5
Soil hydrologic parameters			
Saturated permeability, k_s (mm/hr)		15	65
Saturated volumetric water content, θ_{sat}		0.350	0.323
Residual volumetric water content, θ_r		0.040	0.025
Fitting parameter, α (kPa^{-1})		0.112	0.186
Fitting parameter, n		1.445	1.798
Soil strength parameters			
Internal friction angle, ϕ' (°)		30	36
Cohesion, c' (kPa)		5	0

Figures 2(a) and 2(b). Atterberg's limits, specific gravity of the soil (G_s), strength parameters (ϕ', c'), and the saturated permeability (k_s) are given in Table 2. The studied soils were classified, according to Unified Soil Classification (ASTM D2487), as silty sand (SM) and poorly graded sand with silt (SP-SM). The fine fractions were about 40% for the SM soil and about 10% for the SP-SM soil. The SWC test data were fit using the van Genuchten (VG) equation (van Genuchten 1980) written in Eq. (1) as,
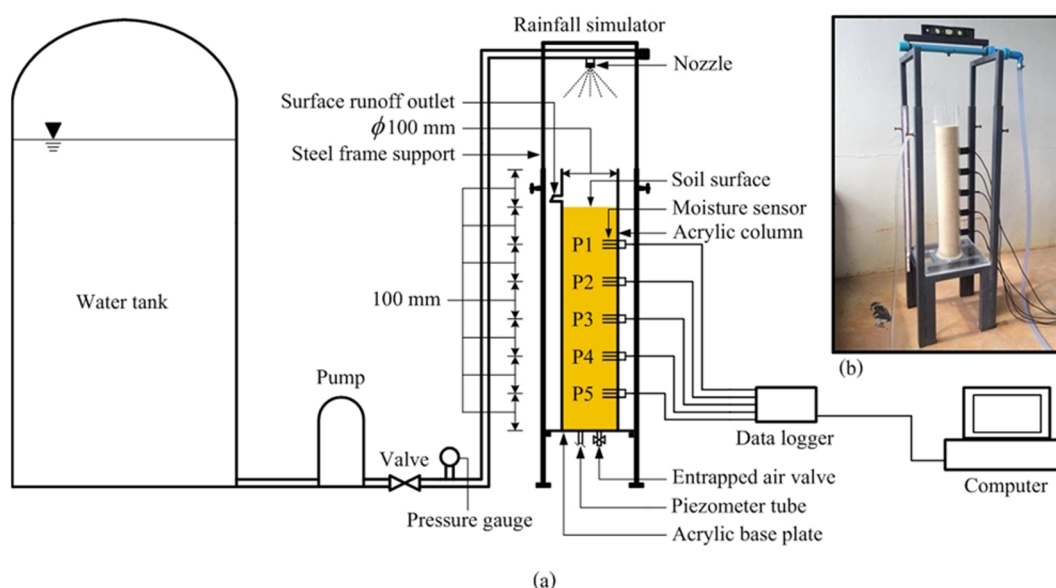

Figure 1 Schematic diagram (a) and photograph (b) of one-dimensional soil column apparatus used in this study.
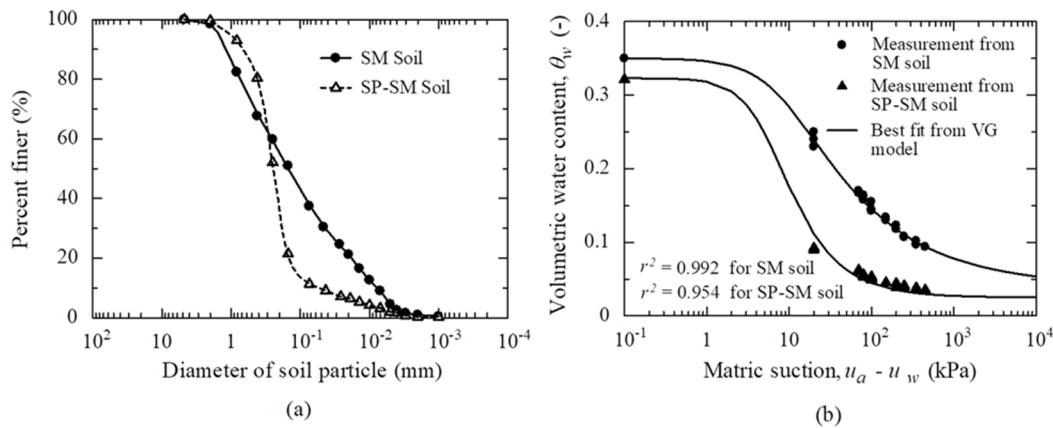
Figure 2 Properties of silty sand (SM) and poorly graded sand with silt (SP-SM) soils used in this study (a) grain size distribution curves and (b) soil water characteristic curves. (r^2, coefficient of determination.)

$$S_e = \frac{\theta_w - \theta_r}{\theta_{sat} - \theta_r} = \left\{ \frac{1}{1 + \left[\alpha\left(u_a - u_w\right)\right]^n} \right\}^{1-1/n} \quad (1)$$

where S_e is the effective degree of saturation, θ_w is water content, θ_r is water content at residual state, θ_{sat} is water content at saturated state, $u_a - u_w$ is matric suction, which is the difference between pore air pressure (u_a) and pore water pressure (u_w), and α and n are VG parameters relating to the inverse of air-entry pressure, and pore size distribution, respectively. The validated VG parameters for the tested soils are given in Table 2.

Table 2 Summary of properties of soils used in this study

Experiment No.	Soil used	γ_d (kN/m³)	i (mm/hr)	i/k_s
1	SM	16.4	5	0.333
2	SM	16.4	10	0.667
3	SM	16.4	20	1.333
4	SM	16.4	45	3.000
5	SP-SM	17.5	10	0.154
6	SP-SM	17.5	20	0.308
7	SP-SM	17.5	45	0.692
8	SP-SM	17.5	70	1.077
9	SP-SM	17.5	100	1.538

Notes: γ_d, dry unit weight; i, rainfall intensity; k_s, saturated permeability; i/k_s, infiltration index.

Figures 3 and 4 respectively present the time series plots of θ_w and the development of the θ_w profile in the SM column subjected to various rainfall intensities. Test results obtained from the SP-SM column (Figures 5 and 6) were similar to those from the SM column. The θ_w responses clearly depended on the magnitude of rainfall intensity and could be classified according to the i/k_s ratio. When $i/k_s < 1.0$, the response of θ_w could be categorized into infiltration and saturation phases. In the infiltration phase, the volumetric water content increased from its initial value (θ_{wi}) to the maximum volumetric moisture content, known as the volumetric water content behind the wetting front (θ_{wb}).

Figure 6 presents the θ_w profile in the SM-SP soil. The value of θ_w changed from θ_{wi} to θ_{wb} within two consecutive probes, which implied the presence of a sharp wetting front. The θ_w profile in SM soil (Figure 4) showed that the θ_w increased immediately from θ_{wi} to an intermediate magnitude of θ_w before slightly increasing again to a final value of θ_{wb}. These results indicated that the wetting front in the SM soil was not as distinct as it was in the SM-SP soil, although the various values of θ_w in the wet zone were very close to θ_{wb}. Soon after the wetting front reached the impervious bottom, the saturation phase began as θ_w, the volumetric water content, increased from θ_{wb} to the saturated water content ($\theta_{sat} = 0.35$). This increase in water content corresponded to the rising of the water table. When $i/k_s \geq 1.0$, θ_w increased from θ_{wi} to $\theta_{sat} = 0.35$ since water started infiltrating into the soil column. Once the
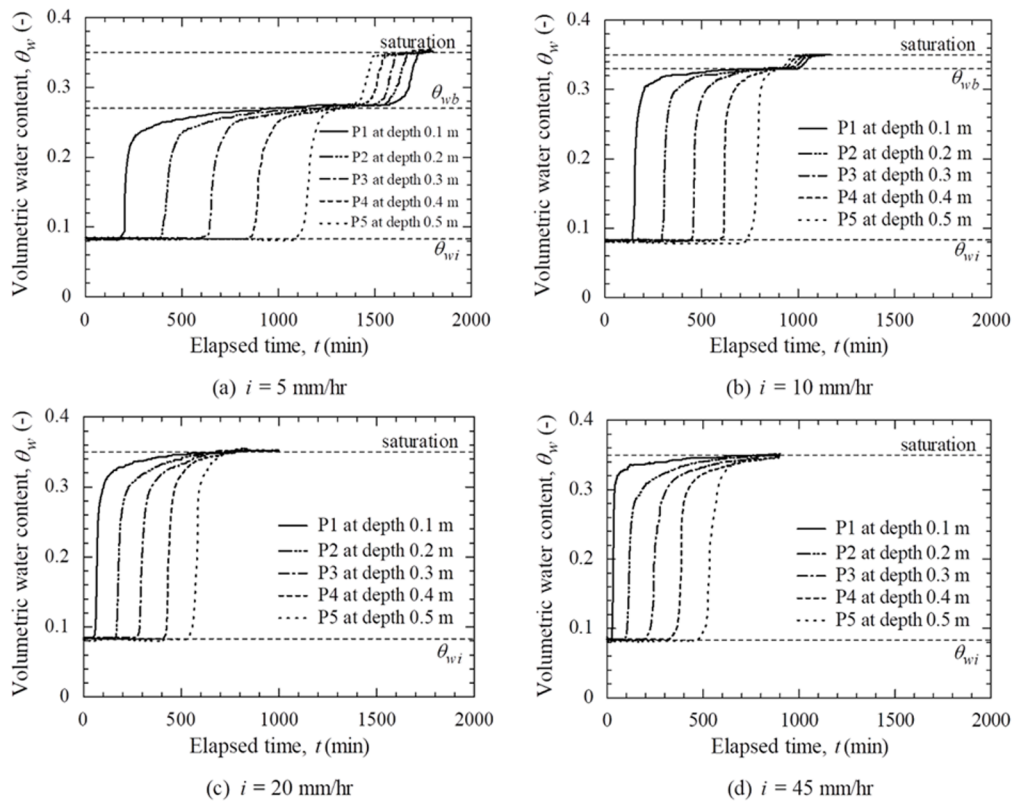
Figure 3 Time series plots of volumetric water content (θ_w) in the silty sand (SM) column for various magnitudes of rainfall intensity (i).
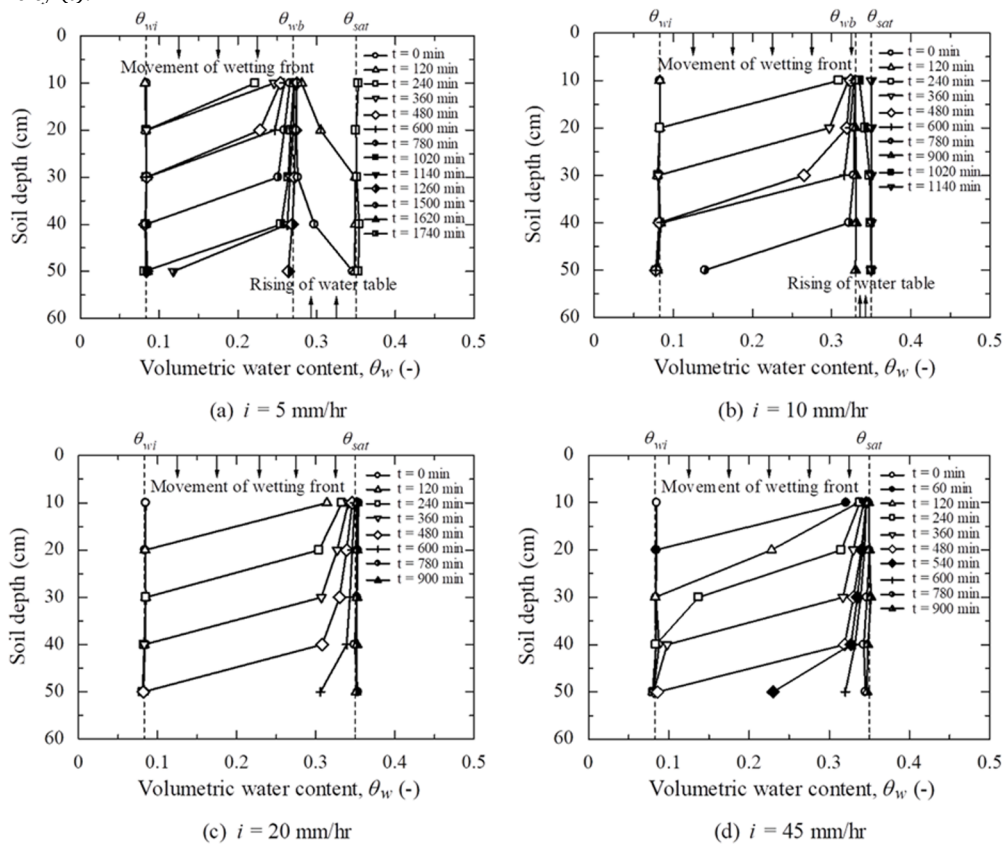

Figure 4 Development of volumetric water content (θ_w) profile in the silty sand (SM) column for various magnitudes of rainfall intensity (i).
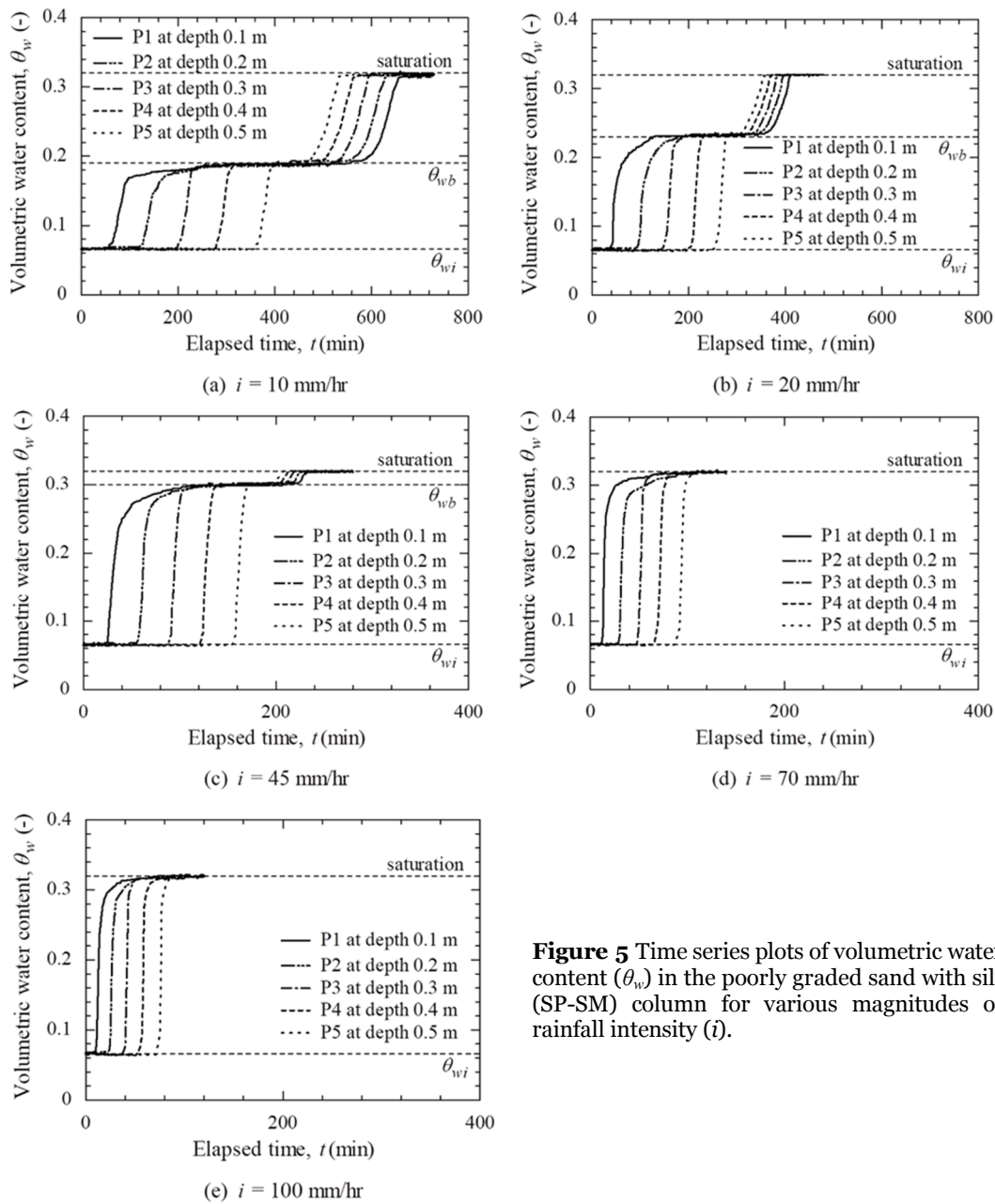
Figure 5 Time series plots of volumetric water content (θ_w) in the poorly graded sand with silt (SP-SM) column for various magnitudes of rainfall intensity (i).

void spaces were fully filled with water, no further increment of θ_w was observed.

1.3 Water Content behind the Wetting Front

As long as rainfall intensity is lower than the soil saturated permeability, the maximum water content during the infiltration process, namely the water content behind the wetting front (θ_{wb}), will be lower than the saturated water content. The unique relationship between θ_{wb} and i/k_s in sandy soil was reported in Chinkulkijniwat et al.

(2016) and modelled as

$$S_{eb} = \frac{\theta_{wb} - \theta_r}{\theta_{sat} - \theta_r} = \left\{ \frac{1}{1 + \left[-\ln\left(i/k_s\right)\right]^n} \right\}^{1-1/n} \quad (2)$$

However, Chinkulkijniwat et al. (2016) validated this model only for a cohesionless sandy soil. Since previous research works (Lee et al. 2011; Chinkulkijniwat et al. 2016; Wu et al. 2017) revealed that the magnitude of θ_{wb} does not depend on the slope angle, we validated Eq. (2) with test data from a one-dimensional infiltration test. Figure 7 presents the relationship found in this
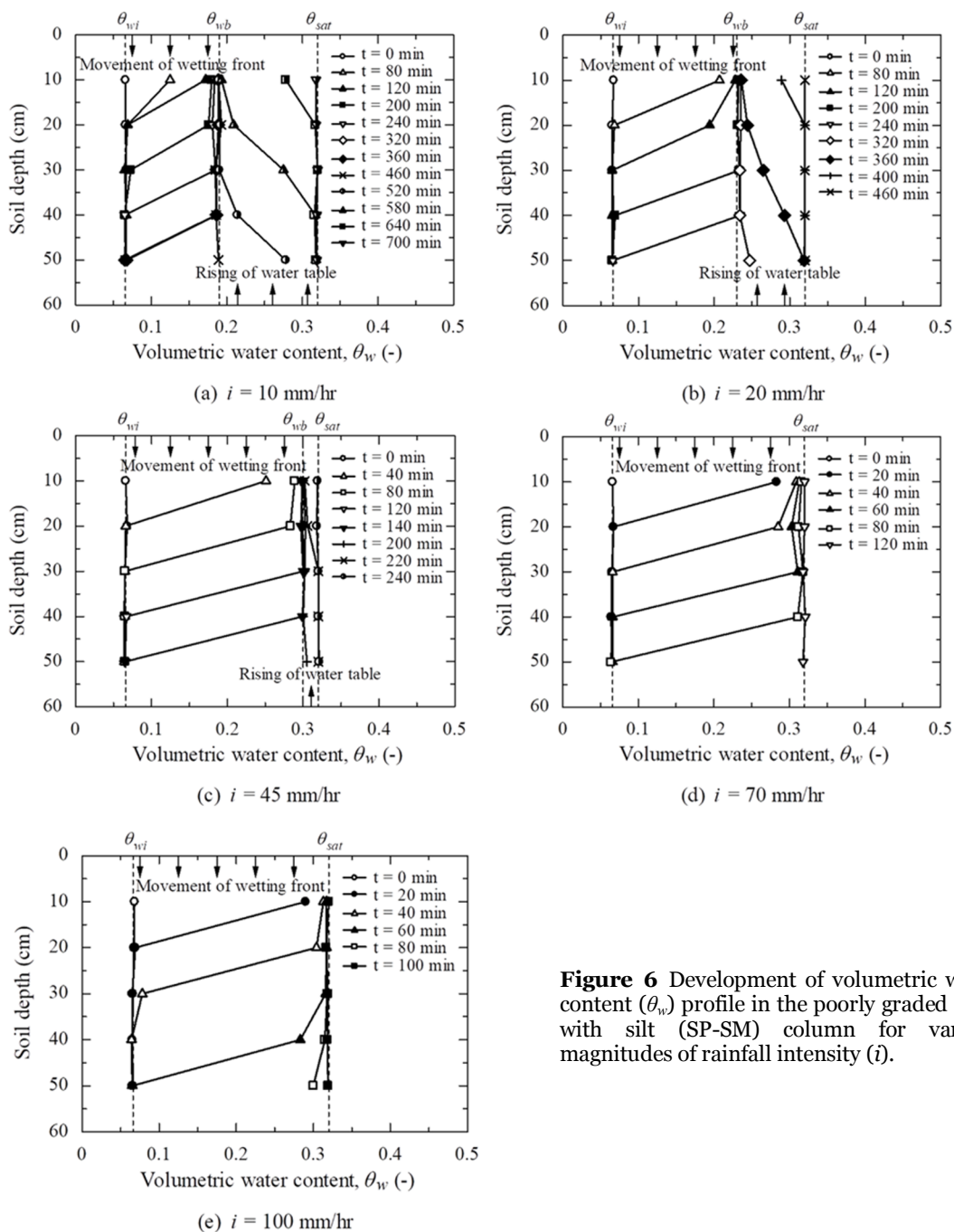
(a) $i = 10$ mm/hr

(b) $i = 20$ mm/hr

(c) $i = 45$ mm/hr

(d) $i = 70$ mm/hr

(e) $i = 100$ mm/hr

Figure 6 Development of volumetric water content (θ_w) profile in the poorly graded sand with silt (SP-SM) column for various magnitudes of rainfall intensity (i).

study between θ_{wb} and i for SM and SP-SM soils. There were 10 and 15 measurements taken in SM and SM-SP soils, respectively. The measured values, taken from 5 TRD probes at each rainfall intensity, were close to each other in both soils, which indicates a unique water content for a particular soil at a given rainfall intensity. Using the van Genuchten parameter values reported in Table 1, the measurements fitted well with Eq. (2), giving an r^2 of 0.996 and 0.997 for the SM and SP-SM soils,

respectively. Therefore, Eq. (2) is valid for the soils studied, which had a certain amount of fine fraction.

2   Analysis of Shallow Landslides

2.1 *FS* at the depth of wetting front's advance

In shallow landslides triggered by rainfall infiltration, the failure has a small depth to length ratio and forms a failure plane parallel to the slope
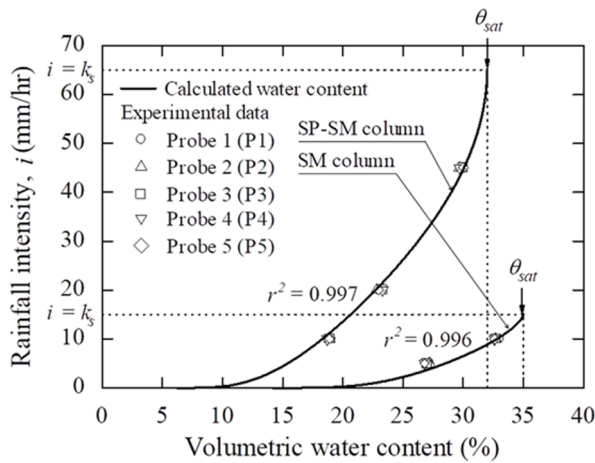
Figure 7 Relationship between volumetric water content behind wetting front (θ_{wb}) and rainfall intensity (i) for silty sand (SM) and poorly graded sand with silt (SP-SM) soils. (r^2, coefficient of determination)

surface. Therefore, infinite slope analysis is justified when assessing the stability of a shallow landslide. The minimum FS is calculated from the depth of wetting penetration. Although the θ_w profile in SM soil did not exhibit a sharp wetting front, the value of θ_w in the wet zone varied very close to θ_{wb}. Therefore, for the sake of simplicity, this study assumes a magnitude of water content in the wet zone equal to θ_{wb}, and hence the minimum FS is at the wetting front.

The FS under vertical seepage and unsaturated conditions is written as (Duncan and Wright 2005)

$$FS = \frac{c' + [\gamma Z \cos^2 \beta - \sigma'_s] \tan \phi'}{\gamma Z \sin \beta \cos \beta}$$
$$= \frac{c' - \sigma'_s \tan \phi'}{\gamma Z \sin \beta \cos \beta} + \frac{\tan \phi'}{\tan \beta} \tag{3}$$

where γ is the unit weight of soil above the wetting front, Z is the particular depth where FS is being calculated, c' is effective cohesion, ϕ' is the effective frictional angle, β is the inclined angle of the slope, and σ'_s is suction stress (Lu and Griffiths 2004; Lu and Likos 2006) defined as

$$\sigma'_s = -\frac{\theta_w - \theta_r}{\theta_{sat} - \theta_r}(u_a - u_w) = -S_e(u_a - u_w) \tag{4}$$

Combining Eq. (2) with Eq. (1), the suction at

the wetting front (expressed as $(u_a - u_w)_b$) is

$$(u_a - u_w)_b = -\frac{1}{\alpha}\ln(i/k_s) \tag{5}$$

Since θ_{wb} can be approximated using Eq. (2), the suction stress at the wetting front can be written as

$$\sigma'_s = \left[-\frac{1}{\alpha}\ln(i/k_s)\right]\left[\frac{1}{1+\left[-\ln\left(i/k_s\right)\right]^n}\right]^{1-1/n} \tag{6}$$

and, therefore, the magnitude of FS at the depth of the wetting front's advance, Z_w, can be calculated by substituting Eq. (3) for the expression of σ'_s in Eq. (6). Figures 8a and 8b respectively present the change of FS with the wetting front's advance Z_w, namely the $FS - Z_w$ plot, in SM and SP-SM soils for slopes of various gradients subjected to various magnitudes of infiltration index (i/k_s). In the SP-SM soil, at every value of i/k_s, the magnitude of FS decreased very rapidly with Z_w, and then leveled off to become asymptotic at the lower limit. In the SM soil, the reduction in FS was slower than in the SP-SM soil. This result suggests that when a wetting front advances at shallow depths, the FS value in SM soil will be higher than the FS value in SP-SM soil.

To investigate the influence of soil properties on the above mentioned characteristics, graphs of FS against Z_w were plotted using varying soil parameters. Figures 9a – 9d present the change of FS with Z_w for various values of the parameters c', ϕ', α, and n. The variation of the parameters c' and ϕ' is presented through lines of different symbols (Figures 9a and 9b), while the variation of the infiltration index is presented through different types of lines (full and dashed lines). At any particular depth of the wetting front's advance, Z_w, the lower the infiltration index was, the greater the FS was. Figure 9a shows clearly that cohesive strength governs the shape of the $FS - Z_w$ plot: the lower the cohesive strength, the sharper the reduction of FS with increasing depth. Thus, the FS value reached the asymptote earlier in soil of a
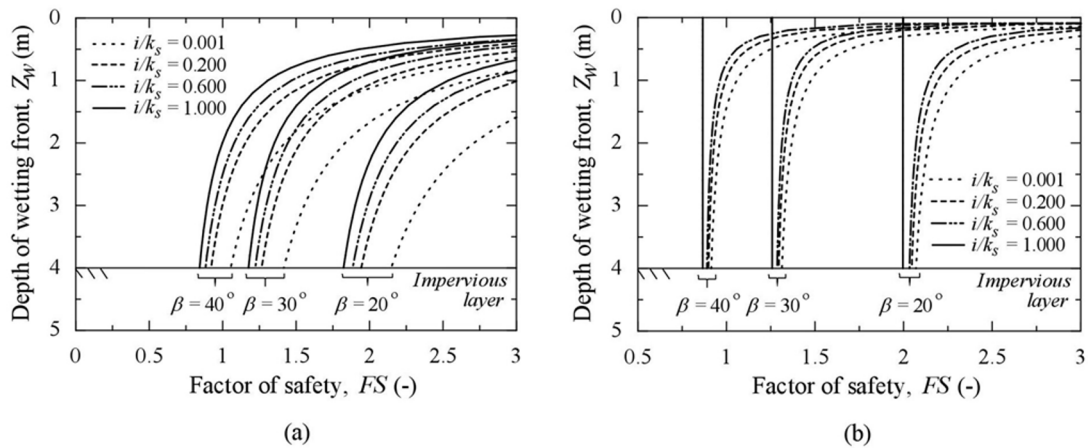
Figure 8 FS-Z_w plots for various magnitudes of infiltration index i/k_s and inclined angle of the slope β in (a) silty sand (SM) soil and (b) poorly graded sand with silt (SP-SM) soil.
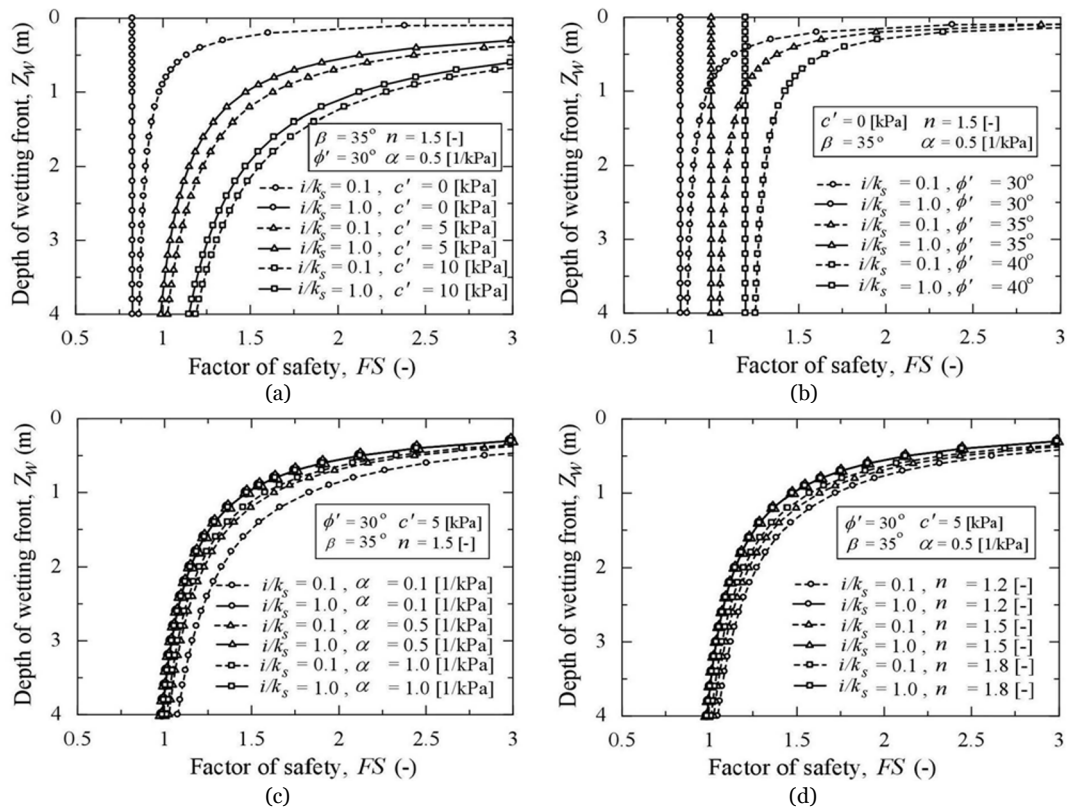

Figure 9 The FS-Z_w plots for various values of the parameters: (a) cohesive strength c', (b) soil frictional angle ϕ', (c) van Genuchten (VG) parameter α, and (d) VG parameter n.

lower cohesive strength than in soil of a higher cohesive strength. With regard to the soil frictional angle, the plots reveal that this factor played no role in the shape of the $FS - Z_w$ plot, changes in the value of the soil frictional angle only resulted in a sideways shift of the plot.

Figures 9c and 9d present the $FS - Z_w$ plots

produced by varying the van Genuchten parameters α and n, respectively. When $i/k_s \geq 1.0$ (full lines), changes of α and n did not affect the $FS - Z_w$ plot since the magnitude of θ_{wb} was equal to the saturated water content and, hence, suction stress, which is a function of the van Genuchten parameter α, and n was completely

eliminated. When $i/k_s < 1.0$ (dash lines), changes in the van Genuchten parameters had less effect on the $FS - Z_w$ plots than the strength parameters did. The greater α and n values yielded $FS - Z_w$ plots with smaller curvatures. Therefore, with identical strength parameters, a sloping ground possessing greater α and n values might exhibit a lower FS at the depth of the wetting front Z_w, particularly when advancing at shallow depths.

2.2 Analysis of critical depth

The critical depth is the depth at which a failure plane is likely to occur and it can be approximated by taking FS to equal 1.0 in Eq. (3). After rearranging the equation, the critical depth can be expressed as

$$Z_{cr} = \frac{c'}{\gamma(1 - A)\sin \beta \cos \beta} - \frac{\sigma'_s \tan \varphi'}{\gamma(1 - A)\sin \beta \cos \beta} \quad (7)$$

where A is the stability index, expressed as $\tan\phi'/\tan\beta$, and Z_{cr} is the critical depth or the depth at which FS is equal to 1.0. Understanding the critical depth characteristic is vital for landslide mitigation and prevention measures, stability reinforcements and the installation of monitoring devices for landslide early warning systems. To characterize the depth of the failure plane, we analyzed a normalized critical depth as a ratio of the critical depth to the depth of the sloping ground (Z_t), as expressed in Eq. (8),

$$\frac{Z_{cr}}{Z_t} = \frac{c'}{\gamma Z_t(1 - A)\sin \beta \cos \beta} - \frac{\sigma'_s \tan \varphi'}{\gamma Z_t(1 - A)\sin \beta \cos \beta} \quad (8)$$

Figure 10 presents the relationships between the normalized critical depth (Z_{cr}/Z_t) and the infiltration index (i/k_s) with various magnitudes of stability index (A) for different values of strength parameters (c' and ϕ') and van Genuchten parameters (α and n). All the plots of

Z_{cr}/Z_t against i/k_s indicate that steep slopes (low A values) yield critical planes at shallow depths (small values of Z_{cr}/Z_t). In cohesionless sloping ground, particularly moderately sloping ground where the gradient was little greater than the soil frictional angle, the critical depth was very sensitive to the rainfall intensity (i/k_s). In cohesive soil, on the other hand, the critical depth was less sensitive to the rainfall intensity. Even a small value of cohesive strength ($c' = 5\,\text{kPa}$) in sloping ground could reduce the sensitivity of the critical depth to rainfall intensity.

A higher α value represents a lower air entry suction, and hence water entry suction. A larger n value represents a more uniform pore size distribution resulting in less suction loss with increments of water content. Typically, coarse grain soil possesses higher α and n values than fine grain soil. The plots of Z_{cr}/Z_t against i/k_s indicate that, for a given i/k_s in sloping ground with larger n and α values, the failure plane should occur at a shallower depth. For cohesive sloping ground, the plot of Z_{cr}/Z_t against i/k_s does not change much with n and α values, whereas the same plot for cohesionless sloping ground does change. For cohesionless sloping ground, larger values of n and α clearly result in a flatter plot of Z_{cr}/Z_t against i/k_s.

3 Conclusions

To verify the unique relationship between θ_{wh} and i/k_s, presented in Chinkulkijniwat et al. (2016), a series of one-dimensional infiltration tests was conducted with silty sand (SM) and poorly graded sand with silt (SP-SM). The stability of these soils in shallow slopes under various rainfall conditions was analyzed. The following conclusions can be made based on this research:

• The unique relationship between θ_{wh} and i/k_s can be formulated either in sandy soil or in soil with a certain amount of fine fraction.

• Strength parameters play a more important role than VG parameters in the variation of FS with the depth of the wetting front's advance.
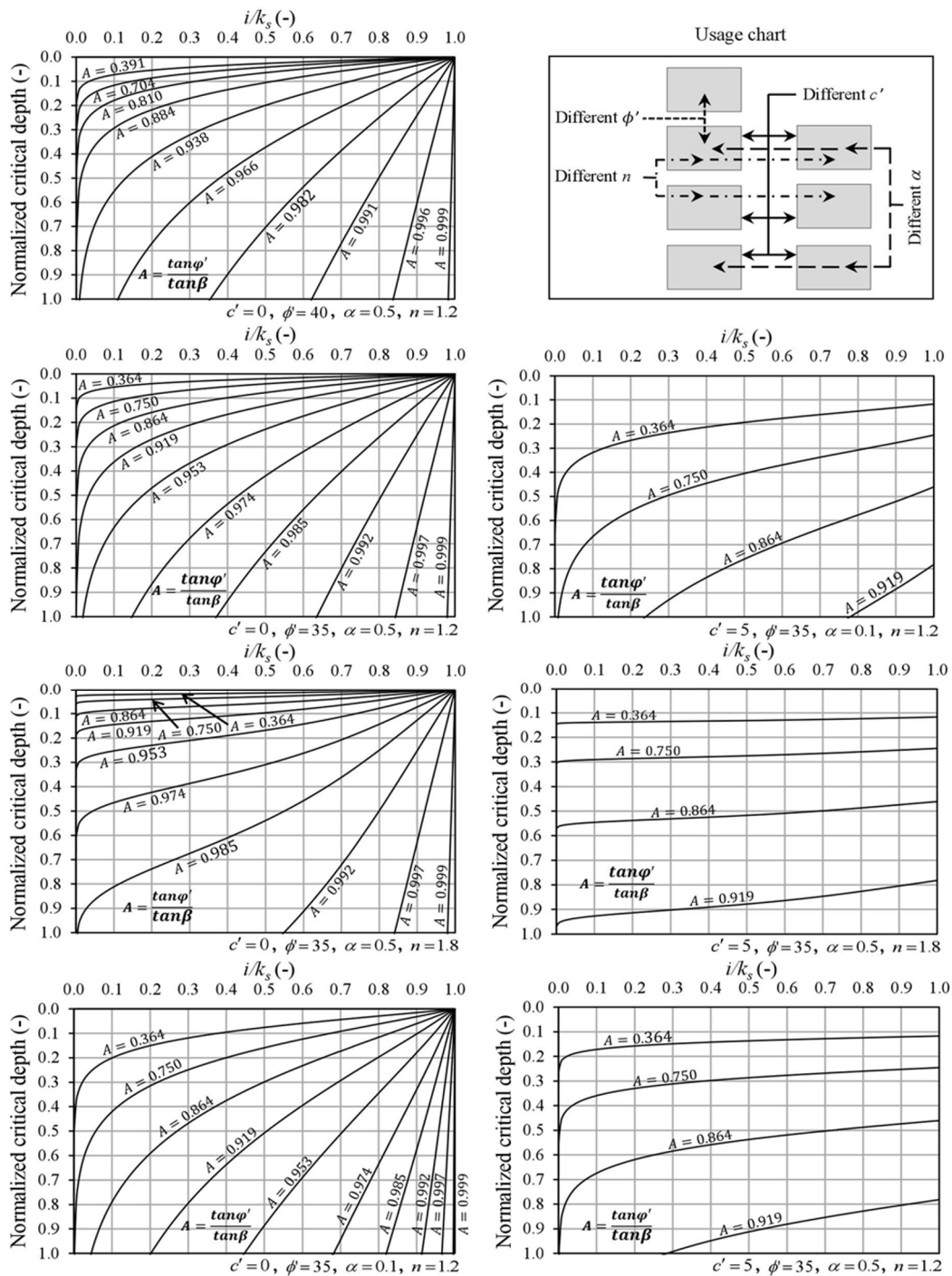
Figure 10 Z_{cr}/Z_t vs. i/k_s plots with various magnitudes of A for different values of strength parameters (c', ϕ') and van Genuchten parameters (α, n).

- For a given i/k_s, lower values of the strength parameters c' and ϕ' result in failure planes at shallower depths.
- In cohesionless sloping ground having a gradient close to the soil frictional angle, when the rainfall intensity approaches the value of the soil saturated permeability, the variation of rainfall intensity plays the major role in the eventual depth of the failure plane.

A little cohesive strength in sloping ground can reduce the influence of rainfall intensity on the depth of a potential failure plane.

Given two soils with identical strength parameters, the more uniformly grained soil which possesses the greater α and n values, tends to fail at a shallower depth.

References

Ali A, Huang J, Lyamin AV, et al. (2014) Simplified quantitative risk assessment of rainfall-induced landslides modelled by infinite slopes. Engineering Geology 179: 102-116. https://doi.org/10.1016/j.enggeo.2014.06.024

Burylo M, Hudek C, Rey F (2011) Soil reinforcement by the roots of six dominant species on eroded mountainous marly slopes (Southern Alps, France). Catena 84: 70-78. https://doi.org/10.1016/j.catena.2010.09.007

Chaminda GPK (2006) Real-time prediction of rain-induced embankment by minimum measurements with back-analysis for SWCC parameters. The University of Tokyo Japan.

Chinkulkijniwat A, Yubonchit S, Horpibulsuk S, et al. (2016) Hydrological responses and stability analysis of shallow slopes with cohesionless soil subjected to continuous rainfall. Canadian Geotechnical Journal 53(12): 2001-2013. https://doi.org/10.1139/cgj-2016-0143

Chu ST (1978) Infiltration during an unsteady rain. Water Resources Research 17(3): 461-466. https://doi.org/10.1029/WR014i003p00461

Duncan JM, Wright SG (2005) Soil strength and slope stability. Scitech Book News; Portland 29(4): 297.

Gabet EJ, Mudd SM (2006) The mobilization of debris flows from shallow landslides. Geomorphology 74: 207-218. https://doi.org/10.1016/j.geomorph.2005.08.013

Green WH, Ampt C A (1911) Studies on soil physics: flow of air and water through soils. Journal of Agriculture Science 4: 1-24. https://doi.org/10.1017/S0021859600001441

Guzzeti F, Peruccacci S, Rossi M, et al. (2008) The rainfall intensity-duration control of shallow landslides and debris flows: an update. Landslides 5: 3–17. https://doi.org/10.1007/s10346-007-0112-1

Lee LM, Kassim A, Gofar N (2011) Performances of two instrumented laboratory models for the study of rainfall infiltration into unsaturated soils. Engineering Geology 117: 78-89. https://doi.org/10.1016/j.enggeo.2010.10.007

Li WC, Lee LM, Cai H, et al. (2013) Combined roles of saturated permeability and rainfall characteristics on surficial failure of homogeneous soil slope. Engineering Geology 153: 105-113. https://doi.org/10.1016/j.enggeo.2012.11.017

Lu N, Griffiths DV (2004) Profiles of steady-state suction stress in unsaturated soils. Journal of Geotechnical and Geoenvironmental Engineering 130(10): 1063-1076. https://doi.org/10.1061/(ASCE)1090-0241(2004)130:10(1063)

Lu N, Likos WJ (2006) Suction stress characteristic curve for unsaturated soil. Journal of Geotechnical and Geoenvironmental Engineering 132(2): 131-142. https://doi.org/10.1061/(ASCE)1090-0241(2006)132:2(131)

Mein RG, Larson CL (1973) Modeling infiltration during a steady rain. Water Resources Research 9(2): 384-394. https://doi.org/10.1029/wr009i002p00384

Naidu S, Sajinkumar KS, Oommen T, et al. (2018) Early warning system for shallow landslides using rainfall threshold and slope stability analysis. Geoscience Frontiers 9(6): 1871-1882. https://doi.org/10.1016/j.gsf.2017.10.008

Postance B, Hillier J, Dijkstra T, et al. (2018) Comparing threshold definition techniques for rainfall induced landslides: a national assessment using radar rainfall. Earth Surface Processes and Landforms 43: 553-560. https://doi.org/10.1002/esp.4202

Shimoma S, Orense R, Honda T, et al. (2002) Model tests on slope failures caused by heavy rainfall. International Congress "INTERPRAEVENT 2002" in the Pacific Rim - Matsumoto, Japan. 2: 547-557.

Tohari A, Nishigaki M, Komatsu M (2007) Laboratory rainfall-induced slope failure with moisture content measurement. Journal of Geotechnical and Geoenvironmental Engineering 133(5): 575-587. https://doi.org/10.1061/(ASCE)1090-0241(2007)133:5(575)

Tosi M (2007) Root tensile strength relationships and their slope stability implications of three shrub species in the northern Apennines (Italy). Geomorphology 87: 268-283. https://doi.org/10.1016/j.geomorph.2006.09.019

Trustrum NA, Gomez B, Page MJ (1999) Sediment production, storage and output: The relative role oflarge magnitude events in steepland catchments. Schweizerbart and Borntraeger science publishers 115: 71-86. https://doi.org/10.1127/zfgsuppl/115/1999/71

Tsai TL, Chen HE, Yang, JC (2008) Numerical modeling of rainstorm-induced shallow landslides in saturated and unsaturated soils. Environmental Geology 55(6): 1269-1277. https://doi.org/10.1007/s00254-007-1075-1

van Genuchten MT (1980) A closed-form equation for predicting the hydraulic conductivity of unsaturated soil. Soil Science Society of America Journal 44: 615-628. https://doi.org/10.2136/sssaj1980.03615995004400050002x

Wu LZ, Zhou Y, Sun P (2017) Laboratory characterization of rainfall-induced loess slope failure. Catena 150: 1-8. https://doi.org/10.1016/j.catena.2016.11.002

Yubonchit S, Chinkulkijniwat A, Horpibulsuk S, et al. (2016). Influence factors involving rainfall-induced shallow slope failure: numerical study. International Journal of Geomechanics 17(7): 04016158. https://doi.org/10.1061/(ASCE)GM.1943-5622.0000865

Yumuang S (2006) 2001 debris flow and debris flood in Nam Ko area, Phetchabun province, central Thailand. Environmental Geology 51(4): 545-564. https://doi.org/10.1007/s00254-006-0351-9

Acknowledgements